Published in "Applied Physics Letters 108(5): 052901, 2016"
which should be cited to refer to this work.

Terahertz ellipsometry study of the soft mode behavior in ultrathin $SrTiO_3$ films

P. Marsik,[a] K. Sen, J. Khmaladze, M. Yazdi-Rizi, B. P. P. Mallett, and C. Bernhard
Department of Physics and Fribourg Center for Nanomaterials, University of Fribourg, Chemin du Musée 3, CH-1700 Fribourg, Switzerland

We present a combined study with time-domain terahertz and conventional far-infrared ellipsometry of the temperature dependent optical response of $SrTiO_3$ thin films (82 and 8.5 nm) that are grown by pulsed-laser deposition on $(La_{0.3}Sr_{0.7})(Al_{0.65}Ta_{0.35})O_3$ (LSAT) substrates. We demonstrate that terahertz ellipsometry is very sensitive to the optical response of these thin films, in particular, to the soft mode of $SrTiO_3$. We show that for the 82 nm film the eigenfrequency of the soft mode is strongly reduced by annealing at 1200 °C, whereas for the 8.5 nm film it is hardly affected. For the latter, after annealing the mode remains at 125 cm^{-1} at 300 K and exhibits only a weak softening to about 90 cm^{-1} at 10 K. This suggests that this ultrathin film undergoes hardly any relaxation of the compressive strain due to the LSAT substrate

Perovskite titanates, particularly in the form of thin films, are important materials for device applications due to their high and tunable dielectric constant. Strontium Titanate ($SrTiO_3$, STO) is a quantum paraelectric material for which the ferroelectric transition is suppressed by the quantum fluctuations of the lattice.[1] The dielectric properties of STO in the static limit and at low frequencies are dominated by a strong polar phonon mode known as the soft mode.[2] In bulk STO, the soft mode eigenfrequency is around 95 cm^{-1} at room temperature and decreases to ~10 cm^{-1} at low temperature. For epitaxial STO films, it was previously shown that this soft mode frequency, and therefore the dielectric constant, can differ substantially.[3–5] Notably, in-plane ferroelectricity near room temperature can be induced in the STO films grown on $DyScO_3$ substrates which introduces a 1% tensile strain.[6,7] On the other hand, the 0.9% compressive strain of a $(La_{0.3}Sr_{0.7})(Al_{0.65}Ta_{0.35})O_3$ (LSAT) substrate causes a sizeable hardening of the soft mode and a corresponding reduction of the in-plane dielectric constant,[8,9] while the out-of-plane dielectric constant diverges.[10] It has also been observed that the strain relaxation, which depends on the thickness of the STO films, and annealing can strongly affect the dielectric properties.[8,11–13]

Terahertz spectroscopic data have been previously reported on the STO films on various substrates (Refs. 4, 5, 8, 9, and 13–17) with thicknesses as low as 17 nm,[4,15] but typically on the order of hundreds of nanometers. The capability of far-infrared and terahertz ellipsometry to detect the soft mode in the STO thin films has already been demonstrated,[3,18] but so far no THz spectra were reported on the ultrathin (~10 nm) films.[19–21]

We show in the following that the combination of a continuous wave Fourier-transform (FTIR) ellipsometry in the far infrared range[22–24] with a time-domain terahertz (TD-THz) ellipsometry[18,25–28] enables one to study the temperature evolution of the in-plane soft mode in thin (82 nm) and even ultrathin (8.5 nm) STO films.

The 82 nm and 8.5 nm thick $SrTiO_3$ films were grown by pulsed laser deposition (PLD) on the LSAT substrates with the dimensions of $10 \times 10 \times 0.5\,mm^3$ and $10 \times 10 \times 3\,mm^3$ (purchased from CrysTec), respectively. They were deposited at 900 °C in a partial pressure 0.12 mbar of O_2 with a laser fluence of 1.4 J/cm^2 and a repetition rate of 2 Hz. The growth was monitored with *in-situ* reflection high electron diffraction (RHEED). Bright RHEED patterns were observed that confirm the smoothness of the film surface. After deposition, the samples were cooled to 700 °C at the rate of 10 °C/min, while the oxygen partial pressure was gradually increased to 1 bar. Subsequently, the temperature was further decreased to room temperature at the rate of 5 °C/min before the samples were removed from the PLD chamber. The thickness of the films was determined *ex-situ* with ellipsometry in the visible range using a Woollam VASE system. Both samples were measured before (as deposited) and after annealing by far-infrared and TD-THz ellipsometry. The *ex-situ* annealing was performed in an ambient atmosphere and the cycle was equal for both samples: After an initial ramp, the temperature was maintained at 300 °C for 2 h, then it was increased to 1200 °C for 4.5 h and was kept for 12 h. The following cool-down from 1200 °C to 200 °C took 6 h.

The far-infrared (75–700 cm^{-1}, 2.2–21 THz) ellipsometry measurements were performed using a home-build ellipsometer attached to a Bruker IFS 113v spectrometer, similar to the setup described in Ref. 22, with a high-pressure Hg-lamp as the light source and a 1.2 K Silicon bolometer detector. This ellipsometer operates in a rotating analyzer (RAE) configuration, with an optional reflection Si-prism compensator that has been used for the range of 75–165 cm^{-1} (2.2–5 THz).[22,24,29]

For the THz range (3–70 cm^{-1}, 0.1–2.1 THz), we used a home-built time-domain THz ellipsometer, which is based on a Menlo Systems C-Fiber 780 nm pulsed laser, with 85 mW output power and 100 fs pulse duration. Figure 1 shows a scheme of the setup. As a THz source, we used an area

[a]Electronic mail: premysl.marsik@unifr.ch

emitter with interdigitated electrodes (LaserQuantum TeraSED)[30] for which the polarization is oriented in the horizontal plane, i.e., in the plane of incidence. The detector is a two-contact LT-GaAs photo-conductive antenna (Menlo Systems TERA8-1) which is also oriented in the plane of incidence. The emitter arm can be rotated to obtain angles of incidence ranging from 45° to 90°. The polarizer and both analyzers are tandems of free standing wire grids (Specac GS57201). The ellipsometers (far-infrared and TD-THz) are equipped with a He-flow optical cryostat (from CryoVac).

The far-infrared ellipsometer is operated in the conventional continuous-wave mode with intensity detection. The analysis is performed with the standard formalism described in Refs. 22, 24, and 31. Time domain spectroscopy, on the other hand, benefits from the ability to obtain the amplitude as well as the phase of the wave arriving at the detector.[32,33] TD-THz ellipsometry was initially proposed to overcome the reference problem of reflection spectroscopy[34,35] and several configurations and approaches have been discussed in the literature.[25–28,36–39] We adopted the scheme used in an FTIR RAE, performing measurements of the full time domain signals for a discrete set of analyzer angles A_j (in our case $A_j = j \times 36°$, with $j = 0, 1, 2, 3, 4$). A second fixed analyzer is required to maintain a constant polarization state of the pulse that is incident on the detector antenna.[38]

In the case of an isotropic sample with Jones matrix[31] elements r_{xx} and r_{yy}, the resulting ellipsometric ratio $\rho = r_{xx}/r_{yy}$ is usually expressed in terms of the ellipsometric angles Ψ and Δ. In the following, we use instead a notation in terms of the complex pseudo-dielectric function:

$$\langle\varepsilon\rangle = \sin^2\varphi\left[1 + \tan^2\varphi\left(\frac{1+\rho}{1-\rho}\right)^2\right], \qquad (1)$$

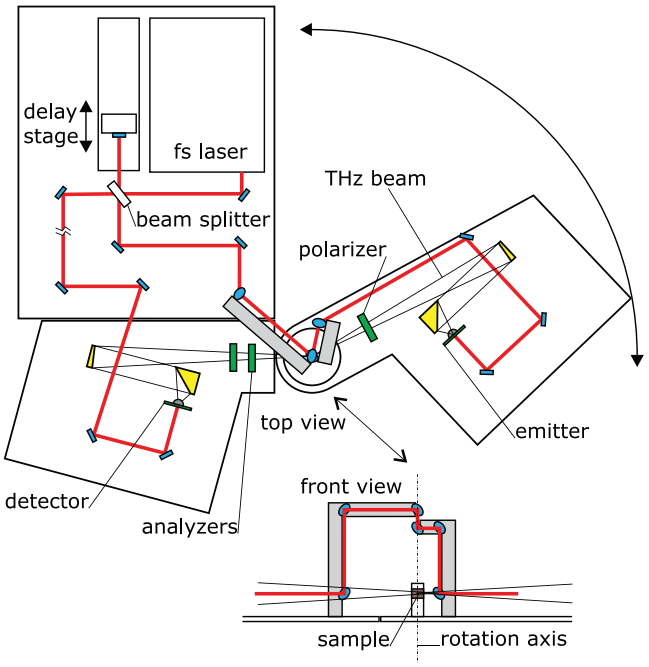

FIG. 1. Schematic top view of the time-domain THz ellipsometer. The sample is located in the axis of rotation of the emitter arm. The front view shows the sample on the cold finger of the cryostat and the geometry of the laser-path bridge between the fixed part and the movable emitter arm.

where φ is the angle of incidence. As will be outlined in the following, here the changes of $\langle\varepsilon\rangle$ with respect to bare substrate $\langle\varepsilon_s\rangle$ are proportional to the optical conductivity of the film. This can be seen by considering an ultrathin film for which $\lambda \gg nd$, with the wavelength of the THz radiation, λ, the film thickness d, and the refractive index, n (with $\varepsilon = N^2 = (n+ik)^2$). The optical response of the ambient/film/substrate system is described with the standard transfer matrix formalism.[31] In the ultrathin limit, the propagation factors in the film, $\exp(\pm i\omega\kappa d/c)$, can be approximated as $1 \pm i\omega\kappa d/c$, with $\kappa = \sqrt{\varepsilon - \sin^2\varphi}$ being the dimensionless normal component of the wave-vector in the film. By omitting terms that are quadratic in d, one obtains analytical expressions for r_p, r_s, and ρ that can be inserted into Eq. (1), to obtain

$$\langle\varepsilon\rangle \doteq \langle\varepsilon_s\rangle - i\omega(\varepsilon - \varepsilon_s)\frac{2dk_s}{c}\frac{\varepsilon - 1}{\varepsilon}\frac{\varepsilon_s}{\varepsilon_s - 1}, \qquad (2)$$

where $\langle\varepsilon_s\rangle$ is the dielectric function of the substrate and $k_s = \sqrt{\varepsilon_s - \sin^2\varphi}$ is the dimensionless normal component of the wave-vector in the substrate.[40]

The second term contains the response of the thin film and it is proportional to the difference between the dielectric functions of the film and the substrate. The first pre-factor $-i\omega$ (except for a missing factor ε_0) converts the difference of $\varepsilon - \varepsilon_s$ to one of the optical conductivities, $\sigma - \sigma_s$, where σ_s is the optical conductivity of the substrate, i.e., $\Delta\sigma = \sigma - \sigma_s = -i\omega\varepsilon_0(\varepsilon - \varepsilon_s)$. The second factor is given by the film thickness, d, scaled by k_s. The factor $(\varepsilon - 1)/\varepsilon$ represents the dielectric contrast between the film and the ambient with $\varepsilon_A = 1$ (it becomes zero for $\varepsilon = 1$ and yields a singularity at $\varepsilon = 0$ that is known as the Berreman mode). Finally, the factor $\varepsilon_s/(\varepsilon_s - 1)$ gives the inverse contrast between the ambient and the substrate, it leads to a singularity at $\varepsilon_s = 1$ which gives rise to a surface guided wave.[41–43] Since the LSAT substrate is transparent in the THz range ($\varepsilon_s \approx 23$), the factor $\varepsilon_s/(\varepsilon_s - 1)$ is about 1.05 and $k_s \approx 4.7$ for $\varphi = 75°$. The large value of the dielectric function of the STO film yields $(\varepsilon - 1)/\varepsilon \approx 1$ and gives rise to a sizeable contrast in $\Delta\sigma$. For example, a conductivity of the STO film of $\sigma_1 = 100\ \Omega^{-1}\text{cm}^{-1}$ at a thickness of $d = 10$ nm yields $\Delta\langle\varepsilon_1\rangle = 0.37$. Note that Eq. (2) is only weakly dependent on the angle of incidence φ through k_s. The highest sensitivity (i.e., the minimum error of $\langle\varepsilon\rangle$) is obtained at the Brewster angle for $\varphi = \varphi_B$ which in case of LSAT with $\varphi_s = 23$ is $\varphi_B = 78.2°$. The ellipsometric measurements presented here have been performed at $\varphi = 75°$. Finally, it should be stressed that the observed contrast, $\varepsilon - \varepsilon_s$, is given by the in-plane response of the film, and thus, the measurements are insensitive to the out-of-plane component of the dielectric function in the possible case of anisotropy of the STO film.

This approach is especially useful in the spectral ranges where the response of the substrate is featureless. For the LSAT substrate, this is the case well below a strong infrared active phonon mode at 158 cm^{-1}. Figures 2(a) and 2(b) clearly show the features of the soft mode of STO which gives rise to a characteristic peak in $\langle\varepsilon_1\rangle \sim \sigma_1$ and a

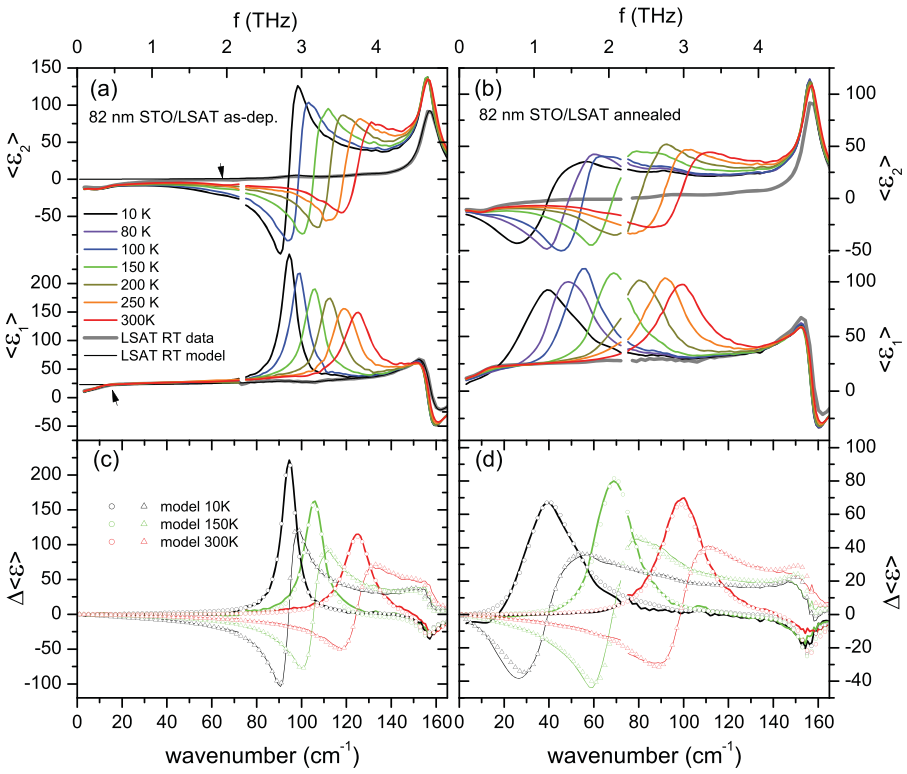

FIG. 2. Pseudo-dielectric functions of the 82 nm thick STO film on LSAT in the as deposited state (a) and the annealed state (b). The data of the bare LSAT substrate are shown by the gray line. The substrate and the film/substrate data deviate from the parameterized model (thin black line) below about 60 cm^{-1} for $\langle\varepsilon_2\rangle$, and about 15 cm^{-1} for $\langle\varepsilon_1\rangle$, as marked by arrows. Difference spectra of $\langle\varepsilon\rangle$ of the as-grown (c) and the annealed (d) film/substrate sample with respect to the substrate at 10 K, 150 K, and 300 K (lines), together with differential model spectra (circles for $\Delta\langle\varepsilon_1\rangle$, triangles for $\Delta\langle\varepsilon_2\rangle$). The color legend applies for all panels.

corresponding resonance feature in $\langle\varepsilon_2\rangle \sim \sigma_2$ that is shifted to lower frequency at low T.

The spectra still contain some features that arise from the polarization dependent diffraction of the light due to the limited sample size. Such effects have been previously discussed for the case of bulk metallic samples in Ref. 44. These diffraction effects occur already in the response of the bare LSAT substrate (gray line in Figs. 2(a) and 2(b)) and can be clearly seen in comparison with the calculated THz response that has been obtained by modelling the phonon modes in the infrared regime with Lorentzian oscillators (thin black line).

These diffraction effects prevent us from analyzing and modelling the measured spectra of $\langle\varepsilon\rangle$. However, since the diffraction effects in the response of the bare substrate and the film/substrate sample are very similar, these are essentially absent in the difference spectra. This is shown in Figs. 2(c) and 2(d) in terms of the difference plots $\Delta\langle\varepsilon(T)\rangle = \langle\varepsilon(T)\rangle - \langle\varepsilon_s(T)\rangle$ for the 82 nm thick STO film in the as grown and the annealed state, respectively.

The $\Delta\langle\varepsilon(T)\rangle$ data are well described by a differential model, which is calculated exactly, using the transfer matrix formalism. The soft mode of STO is well accounted for by a single Lorentzian oscillator $\varepsilon(\omega) = \varepsilon_\infty + 4\pi F^2\omega_0^2/(\omega_0^2 - \omega^2 - i\omega\gamma)$. For the as grown 82 nm thick STO film, the modelling yields a relatively sharp soft mode which at 300 K is centered at 126 cm^{-1} with a width, γ, of about 20 cm^{-1}. With the decreasing temperature, it exhibits a fairly weak softening to 95 cm^{-1} at 10 K, comparable to previous reports.[9] In the annealed state, the soft mode frequency is considerably lower and the T-dependent softening is much stronger, i.e., the eigenfrequency decreases from about 100 cm^{-1} at 300 K to about 40 cm^{-1} at 10 K. The soft mode is also considerably broader than in the as grown state with $\gamma \sim 30$ cm^{-1} at 300 K and 35 cm^{-1} at 10 K. The structure near 155 cm^{-1} is a remnant of the LSAT phonon, which, according to Eq. (2), modifies the contrast between the film and the substrate.

In the case of the as grown 82 nm film, below 100 K, two oscillators with similar eigenfrequencies ω_0 but different γ values improve the fit quality. This inhomogeneous broadening of the soft mode seems related to the antiferrodistortive phase transition from a cubic to a tetragonal structure which occurs in bulk $SrTiO_3$ at 105 K.[45]

The strong reduction of the soft mode frequency due to a high temperature annealing treatment is in agreement with previous reports from THz transmission measurements of a 370 nm thick STO film on the LSAT.[8] Possible explanations are in terms of a relaxation of the strain state in large parts of such thick films or a removal of defects and vacancies that are also known to cause a hardening of the STO soft mode.

This raises the question whether a similar annealing-induced effect on the soft mode occurs in the epitaxial STO films which are too thin to exhibit a large strain relaxation and thus remain clamped to the substrate. Thanks to the high sensitivity of the differential approach discussed above, we were able to observe the soft mode behavior in a 8.5 nm thick STO film on the LSAT.

The as-deposited sample was studied with ellipsometry only at room temperature (data not shown). After the high temperature annealing treatment, the THz and infrared ellipsometry measurements have been performed as a function of temperature, as shown in Figure 3 in terms of the differential data. Despite the much smaller signal, the characteristic features of the soft mode, such as the peak in $\Delta\langle\varepsilon_1\rangle \sim \sigma_1$ and the resonance feature in $\Delta\langle\varepsilon_2\rangle \sim \sigma_2$, are still clearly discernible. It is also evident that the dispersion of the soft mode is rather weak, i.e., it softens from about 128 cm^{-1} at 300 K to 96 cm^{-1} at 10 K. In comparison, in the as-deposited state the soft mode

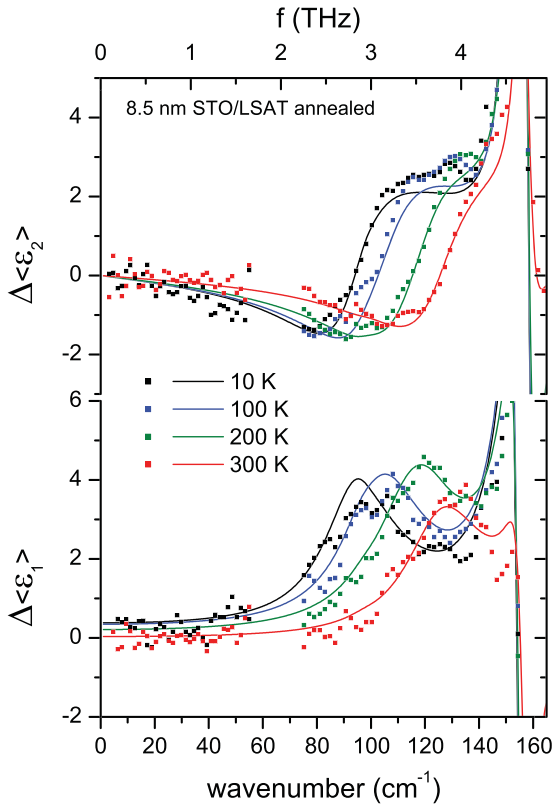

FIG. 3. Differential pseudo-dielectric function of the 8.5 nm thin STO film with respect to the bare LSAT substrate.

frequency at 300 K was at 132 cm^{-1}. For this ultrathin and fully strained STO thin film, the high temperature annealing treatment has hardly influenced the position of the soft mode, and the broadening however increased from about 20 to 37 cm^{-1}.

The overview of the temperature dependencies of the in-plane soft mode eigenfrequency and its broadening for the two STO films in the as grown and the annealed state is shown in Figures 4(a) and 4(b), respectively. Also shown are the literature data for bulk STO.[4] Figure 4(c) shows a comparison of the soft mode response at 300 K in terms of the modelled spectra.

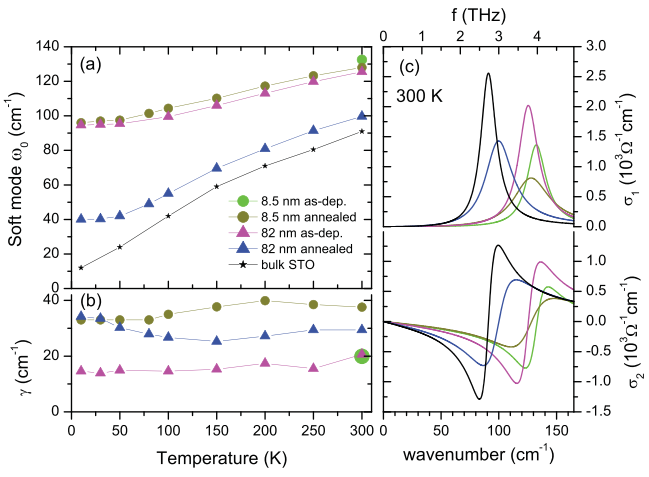

FIG. 4. Temperature dependence of the STO in-plane soft mode frequency, ω_0 (a), and the broadening, γ (b). Model fits of the optical conductivity at 300 K (c), with the same legend as (a). Bulk STO values from Ref. 4.

In summary, we have shown that in the ultrathin film limit, the directly measured ellipsometric data expressed in the form of pseudo-dielectric functions can be readily interpreted as the sum of the dielectric function of the substrate (particularly in the range of its transparency) and the optical conductivity of the film. Both the film/substrate and the bare substrate data exhibit diffraction artefacts due to the limited sample size. These are removed in the differential pseudo-dielectric spectra, which can be subsequently analyzed with a differential model. We applied this approach on thin and ultrathin films of $SrTiO_3$ deposited on the LSAT substrates and observed the temperature dependence of the soft mode dispersion. For the 82 nm thick STO film, we observed a significant effect of the annealing treatment on the eigenfrequency of the soft phonon mode that was absent for the 8.5 nm film. This suggests that the strain due to the LSAT substrate can be readily maintained in such an ultrathin STO film.

This work has been supported by the Schweizer Nationalfonds (SNF) through the Grant No. 200020-153660 and by the Sciex-NMS^{CH} Grant No. CZ0908003. We acknowledge the helpful discussions with Thomas Feurer, Andreas Bitzer, Florian Enderli, Gregory Gäumann, and Matthias Rössle.

[1] K. A. Müller and H. Burkard, Phys. Rev. B **19**, 3593 (1979).
[2] J. Petzelt, S. Kamba, and J. Hlinka, in *New Developments in Advanced Functional Ceramics 2007*, edited by L. Mitoseriu (Transworld Res. Net., 2007), Chap. 14, pp. 387–421, ISBN: 81-7895-248-3.
[3] A. A. Sirenko, C. Bernhard, A. Golnik, A. M. Clark, J. Hao, W. Si, and X. X. Xi, Nature **404**, 373 (2000).
[4] I. Fedorov, V. Zelezny, J. Petzelt, V. Trepakov, M. Jelinek, V. Trtik, M. Cernansky, and V. Studnicka, Ferroelectrics **208–209**(1), 413–427 (1998).
[5] T. Ostapchuk, J. Petzelt, V. Zelezny, A. Pashkin, J. Pokorny, I. Drbohlav, R. Kuzel, D. Rafaja, B. P. Gorshunov, M. Dressel, Ch. Ohly, S. Hoffmann-Eifert, and R. Waser, Phys. Rev. B **66**, 235406 (2002).
[6] J. H. Haeni, P. Irvin, W. Chang, R. Uecker, P. Reiche, Y. L. Li, S. Choudhury, W. Tian, M. E. Hawley, and B. Craigo, Nature **430**, 758 (2004).
[7] V. Skoromets, C. Kadlec, J. Drahokoupil, J. Schubert, J. Hlinka, and P. Kuzel, Phys. Rev. B **89**, 214116 (2014).
[8] I. Katayama, H. Shimosato, D. S. Rana, I. Kawayama, M. Tonouchi, and M. Ashida, Appl. Phys. Lett. **93**, 132903 (2008).
[9] D. Nuzhnyy, J. Petzelt, S. Kamba, T. Yamada, M. Tyunina, A. K. Tagantsev, J. Levoska, and N. Setter, J. Electroceram. **22**, 297–301 (2009).
[10] A. Verma, S. Raghavan, S. Stemmer, and D. Jena, Appl. Phys. Lett. **107**, 192908 (2015).
[11] F. He, B. O. Wells, and S. M. Shapiro, Phys. Rev. Lett. **94**, 176101 (2005).
[12] Z. Y. Zhai, X. S. Wu, H. L. Cai, X. M. Lu, J. H. Hao, Ju Gao, W. S. Tan, Q. J. Jia, H. H. Wang, and Y. Z. Wang, J. Phys. D: Appl. Phys. **42**, 105307 (2009).
[13] R. Kinjo, I. Kawayama, H. Murakami, and M. Tonouchi, Adv. Mater. Phys. Chem. **3**, 58–61 (2013).
[14] C. Kadlec, V. Skoromets, F. Kadlec, H. Nemec, J. Hlinka, J. Schubert, G. Panaitov, and P. Kuzel, J. Phys. Condens. Matter **21**, 115902 (2009).
[15] D. Nuzhnyy, J. Petzelt, S. Kamba, X. Marti, T. Cechal, C. M. Brooks, and D. G. Schlom, J. Phys. Condens. Matter **23**, 045901 (2011).
[16] I. Katayama, H. Aoki, J. Takeda, H. Shimosato, M. Ashida, R. Kinjo, I. Kawayama, M. Tonouchi, M. Nagai, and K. Tanaka, Phys. Rev. Lett. **108**, 097401 (2012).
[17] R. Kinjo, I. Kawayama, H. Murakami, and M. Tonouchi, J. Infrared Millimeter Terahertz Waves **33**, 67–73 (2012).
[18] N. Matsumoto, T. Hosokura, T. Nagashima, and M. Hangyo, Opt. Express **36**, 265 (2011).
[19] J. F. O'Hara, W. Withayachumnankul, and I. Al-Naib, J. Infrared Millimeter Terahertz Waves **33**, 245 (2012).
[20] M. Tyunina, J. Narkilahti, J. Levoska, D. Chvostova, A. Dejneka, V. Trepakov, and V. Zelezny, J. Phys. Condens. Matter **21**, 232203 (2009).

[21]C. Cen, M. P. Warusawithana, and J. Levy, Ann. Phys. (Berlin) **524**, 429 (2012).
[22]C. Bernhard, J. Humlicek, and B. Keimer, Thin Solid Films **455–456**, 143 (2004).
[23]T. Hofmann, U. Schade, C. M. Herzinger, P. Esquinazi, and M. Schubert, Rev. Sci. Instrum. **77**, 063902 (2006).
[24]K. Kanehara, T. Hoshina, H. Takeda, and T. Tsurumi, Appl. Phys. Lett. **105**, 042901 (2014).
[25]T. Nagashima and M. Hangyo, Appl. Phys. Lett. **79**, 3917 (2001).
[26]N. Matsumoto, T. Fujii, K. Kageyama, H. Takagi, T. Nagashima, and M. Hangyo, Jpn. J. Appl. Phys. **48**, 09KC11 (2009).
[27]M. Neshat and N. P. Armitage, Opt. Express **20**, 29063 (2012).
[28]C. M. Morris, R. Valdes-Aguilar, A. V. Stier, and N. P. Armitage, Opt. Express **20**, 12303 (2012).
[29]T. Hoshina, K. Kanehara, H. Takeda, and T. Tsurumi, Jpn. J. Appl. Phys. **53**, 09PD03 (2014).
[30]A. Dreyhaupt, S. Winnerl, T. Dekorsy, and M. Helm, Appl. Phys. Lett. **86**, 121114 (2005).
[31]*Handbook of Ellipsometry*, edited by H. Tompkins and E. Irene (William Andrew Publishing, New York, 2005).
[32]*Terahertz Spectroscopy: Principles and Applications*, edited by S. Dexheimer (Taylor & Francis Group, 2008).
[33]D. Grischkowsky, S. Keiding, M. van Exter, and Ch. Fattinger, J. Opt. Soc. Am. B **7**, 2006 (1990).
[34]T. I. Jeon and D. Grischkowsky, Appl. Phys. Lett. **72**, 3032 (1998).
[35]A. Pashkin, M. Kempa, H. Nemec, F. Kadlec, and P. Kuzel, Rev. Sci. Instrum. **74**, 4711 (2003).
[36]M. Khazan, R. Meissner, and I. Wilke, Rev. Sci. Instrum. **72**, 3427 (2001).
[37]Y. Ino, R. Shimano, Y. Svirko, and M. Kuwata-Gonokami, Phys. Rev. B **70**, 155101 (2004).
[38]O. Morikawa, A. Quema, S. Nashima, H. Sumikura, T. Nagashima, and M. Hangyo, J. Appl. Phys. **100**, 033105 (2006).
[39]D. K. George, A. V. Stier, C. T. Ellis, B. D. McCombe, J. Cerne, and A. G. Markelz, J. Opt. Soc. Am. B **29**, 1406 (2012).
[40]D. E. Aspnes, Thin Solid Films **89**, 249–262 (1982).
[41]D. W. Berreman, Phys. Rev. **130**, 2193 (1963).
[42]M. Schubert, *Infrared Ellipsometry on Semiconductor Layer Structures* (Springer-Verlag, Berlin, Heidelberg, 2004).
[43]A. Dubroka, M. Rössle, K. W. Kim, V. K. Malik, L. Schultz, S. Thiel, C. W. Schneider, J. Mannhart, G. Herranz, O. Copie, M. Bibes, A. Barthélémy, and C. Bernhard, Phys. Rev. Lett. **104**, 156807 (2010).
[44]J. Humlicek and C. Bernhard, Thin Solid Films **455–456**, 177 (2004).
[45]F. W. Lytle, J. Appl. Phys. **35**, 2212 (1964).